



Effect of Cu content on the microstructure, mechanical and corrosion behavior of AlFeNiMnCu_x high-entropy alloys

Linjiansheng Zhao ^a, Chenran Xu ^a, Liyang Fang ^{a,b}, Hongqun Tang ^c, Yifang Ouyang ^a, Xiaoma Tao ^{a,c,*}

^a School of Physical Science and Technology, Guangxi Key Laboratory for Relativistic Astrophysics, Guangxi Colleges and Universities Key Laboratory of Blue Energy and Systems Integration, Guangxi University, Nanning 530004, PR China

^b Nanning Engineering Technology Research Center for Power Transmission System of New Energy Vehicle, College of Traffic and Transportation, Nanning University, Nanning 530200, PR China

^c State Key Laboratory of Featured Metal Materials and Life-cycle Safety for Composite Structures, School of Resources, Environment and Materials, Guangxi University, Nanning 530004, PR China



ARTICLE INFO

Keywords:

High entropy alloy
Microstructure
Mechanical property
Corrosion resistance

ABSTRACT

The microstructure, mechanical and corrosion behavior of AlFeNiMnCu_x ($x = 0.5, 0.75, 1.0, 1.25$) high-entropy alloys (HEAs) have been investigated. It is identified as the BCC solid solution. An increase in concentration of Cu promotes the formation of reinforced phases and increases solid solution strengthening, which enhances mechanical properties. Additionally, the incorporation of Cu results in the formation of FCC structures, which in turn facilitates the transformation of corrosion modes and thus inhibits the corrosion. Among the studied HEAs, AlFeNiMnCu HEA ($x = 1.0$) is particularly noteworthy on mechanical properties, exhibiting a yield strength of 1559 MPa, a fracture strength of 1699 MPa, a plastic strain of 14.3 %, and a Vickers hardness of 563 HV. And AlFeNiMnCu HEA also exhibits excellent performance in electrochemical corrosion, as indicated by an E_{corr} of -678.5 mV and an I_{corr} of 22.7 $\mu\text{A}/\text{cm}^2$. The results demonstrate that an increase in the Cu content has significant implications for microstructure, mechanical and corrosion behavior.

1. Introduction

Recently, the existence of a new class of materials has been defined, as the mixing entropy of these materials obtained by thermodynamic calculations are above 1.5 R [1–3], namely high entropy alloys (HEAs) proposed by Yeh et al. [1] and Cantor et al. [4]. There are four core effects in HEAs [5–8], that is, the high entropy effect, the sluggish diffusion effect, the lattice distortion effect and the “cocktail” effect. HEAs exhibit high mixing entropy, which makes it inclined to generate simple solid solution structures, such as BCC, FCC and HCP. Therefore, HEAs exhibit superior mechanical and corrosion resistance compared to traditional alloys [9,10], and HEAs are generally regarded as prospective structural materials [9–11].

The initial generation of HEAs is represented by CoCrFeMnNi alloys [12]. To date, numerous HEAs design solutions continue to be based on the CoCrFeMnNi system [13–17]. However, a number of these HEAs demonstrate inadequate mechanical strength, in order to improve the

strength, some methods have been performed [18–20]. Recently, the Al-containing HEAs have been the focus of extensive research, which has demonstrated that the addition of Al enhances the strength and hardness through the formation of BCC structures [21–24]. Meanwhile, with the increasing strength and hardness, the plasticity of HEAs display poor [17,25–27].

Recent researches have demonstrated that Cu has a significant impact on the microstructure, mechanical properties and corrosion resistance of HEAs. The addition of Cu to HEAs has been demonstrated to facilitate the formation of FCC structures and refine the grain [28], which can enhance the plasticity [29,30]. This phenomenon can be attributed to the fact that the FCC crystal structure possesses a greater number of slip systems. Additionally, an increase in the volume fraction of the FCC phase can enhance the passivation ability [31,32]. Conversely, one study has demonstrated that an increase in Cu content facilitates the formation of a Cu-rich passive film, which inhibits the transport of iron at grain boundaries [33]. Those results show that the

* Corresponding author at: School of Physical Science and Technology, Guangxi Key Laboratory for Relativistic Astrophysics, Guangxi Colleges and Universities Key Laboratory of Blue Energy and Systems Integration, Guangxi University, Nanning 530004, PR China.

E-mail address: [taoxtoma@gxu.edu.cn](mailto:taoxiaoma@gxu.edu.cn) (X. Tao).

Cu element can be used to stabilize the FCC phase and facilitate the formation of a passive film, and which can optimize the mechanical properties and corrosion resistance of HEAs. Additionally, quite a lot of studies show that the Co/Cr-containing HEAs trend to result in the generation of numerous complex phases [13,34–37], which has a detrimental impact on the properties.

Consequently, this work will focus on mechanical properties and corrosion resistance of AlFeNiMnCu_x HEAs, which is considered as the replacement of the Cr and Co in CoCrFeMnNi alloys with Cu and Al. The design solution takes full advantage of Al-containing and Cu-containing HEAs, which is expected to give the HEAs excellent strength and plasticity through the structural optimization, as well as good corrosion resistance. Effect of Cu content on the microstructure, mechanical properties and corrosion resistance of AlFeNiMnCu_x ($x = 0.5, 0.75, 1.0, 1.25$) HEAs will be studied. The results can contribute to the design of Cu-containing HEAs with excellent mechanical properties and corrosion resistance for application in structural materials.

2. Experimental sections

2.1. Material preparation

Raw metal materials (Al, Fe, Ni, Mn and Cu particles) with the purity of 99.9 wt% were used to synthesize HEAs. Composition of AlFe-NiMnCu_x HEAs was listed in Table 1. The button ingots of samples were prepared by vacuum arc melting. To avoid losses during the melting process, the volatile raw materials were added to the bottom of the copper crucible. During melting HEAs, the ingots were turned and remelted repeatedly more than five times to ensure chemical homogeneity. Subsequently, the samples were processed by a wire-cut electric discharge machine for the subsequent examination. For convenience, the AlFeNiMnCu_x ($x = 0.5, 0.75, 1.0, 1.25$) HEAs denoted as Cu0.5, Cu0.75, Cu1.0 and Cu1.25.

2.2. Materials characterizations

All samples were polished and cleaned with ultrasound to remove the surface oxides prior to testing. The crystal structure of powders was characterized by an X-ray diffractometer (XRD, Smart Lab 3 KW, Rigaku, JPN) with Cu K α radiation. The microstructure and elemental distribution were examined by electron probe microanalysis (EPMA, JXA-8230, JEOL, JPN) with wave dispersive spectroscopy (WDS), and transmission electron microscopy (TEM, Tecnai G2 F20, FEI, US) with energy dispersive spectroscopy (EDS).

2.3. Mechanical property measurement

The compression experiment was conducted using a universal testing machine (INSTRON-8801, Instron, US) at room temperature. And rectangular sample with dimensions of $5 \times 5 \times 10$ mm was used. Vickers hardness was determined by means of a Vickers hardness instrument (Q30A, Qness, AUS) with a load of 9.8 N applied for 10 s. The density was determined by the Archimedes' principle. All values of mechanical properties were obtained using average value from testing at five times.

Table 1
Composition of the HEAs (at%).

Alloys	Al	Fe	Ni	Mn	Cu
Cu0.5	22.22	22.22	22.22	22.22	11.12
Cu0.75	21.05	21.05	21.05	21.05	15.80
Cu1.0	20.00	20.00	20.00	20.00	20.00
Cu1.25	19.05	19.05	19.05	19.05	23.80

2.4. Corrosion behavior measurement

Electrochemical tests were conducted using an electrochemical workstation (Reference 600, Gamry, US) in 3.5 wt% NaCl solution at room temperature. Prior to testing, the samples to be polished were immersed in the solution for 3 h to ensure chemical balance and to obtain a stable open circuit potential (OCP). The potentiodynamic polarization tests were performed using a three-electrode electrochemical cell, with the sample as the working electrode, a saturated Ag/AgCl electrode as the reference electrode, and a platinum sheet as the auxiliary electrode. The potentiodynamic polarization behavior was carried out from -0.5 V to 1.0 V with a scanning rate of 1 mV/s. Electrochemical impedance spectroscopy (EIS) measurements were performed at OCP using an applied alternating current signal with a perturbation signal of 5 mV and a frequency range of 10^5 Hz to 10^{-2} Hz. To confirm the reproducibility of data, the electrochemical tests were repeated five times.

3. Results and discussion

3.1. Structural characterization

XRD results are presented in Fig. 1, and the corresponding phase information is given in Table S1. From a holistic perspective, the AlFe-NiMnCu_x HEAs are composed of BCC phases. As the Cu content increased, the formation of FCC peaks was observed, resulting in outcomes that are comparable to those observed in other Cu-containing HEAs [38,39]. For Cu0.5, the diffraction peaks of BCC are needed, with a slight diffraction peak of B2 appearing at approximately 31° of 20. For Cu0.75, the formation of more B2 structures is found in Fig. 1(b) and corroborated in Table S1. This may be attributed to an increase in B2-compounds, caused by an interaction between Al and other atoms displaced by Cu. This phenomenon can be attributed to the replacement of the other atoms by Cu, resulting in the formation of substitutional solid solution [40]. The substitutional solid solution is the process by which atoms of similar radius are incorporated into the crystal structure to replace other atoms, and is commonly found in HEAs of similar atomic radius (see in Table 2). Additionally, the BCC and B2 peaks are observed to separate, which suggests that the lattice distortion has occurred. Given the high positive enthalpy exhibited by Cu in interaction with other atoms (see in Table 3), the formation of FCC structures is found, which corresponds to FCC1 peaks (see in Fig. 1(b)). As the Cu content increased further ($x = 1.0, 1.25$), two sets of adjacent diffraction peaks of FCC1 and FCC2 are observed and the diffraction peaks of FCC1 become more prominent, which indicates the presence of significant Cu segregation.

The back scattered electron (BSE) images and WDS maps are shown in Fig. 2 (BSE images enlargement see in Fig. S1). As illustrated in BSE images, the microstructure exhibits a typical dendrite and inter-dendrite. The structures are identified as light inter-dendritic regions (IR) and dark dendritic regions (DR). As illustrated in WDS maps, the DR show enrichment of Al, Fe and Ni and the IR show enrichment of Cu, uniform Mn distribution. Additionally, the boundary between Cu and Fe becomes apparent with an increase in Cu content, which identifies the elemental segregation due to the high positive enthalpy between Cu and Fe (see in Table 3) [9].

In order to gain further insight, the TEM results obtained from the Cu0.5 and Cu1.25 are presented in Figs. 3 and 4, respectively. In the case of Cu0.5, rod-like structures are observed in the TEM micrograph (Fig. 3 (a)), which exhibits a homogeneous distribution. As illustrated in Fig. 3 (b), the microstructure is identified as the BCC solid solution based on the selected area electron diffraction (SAED), which corresponds to the diffraction peaks of B2 and BCC in the XRD result. Furthermore, the HRTEM image (Fig. 3(c)) demonstrates the detailed information of the rod-like structures, which indicates that the rod-like precipitates of disordered BCC structures are surrounded by few ordered B2 and

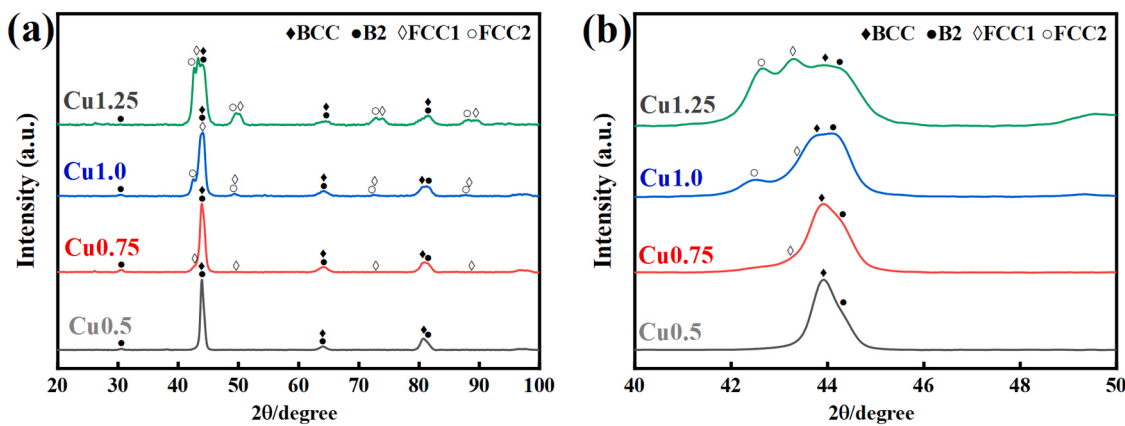


Fig. 1. (a) XRD results and (b) the enlarged region of angles.

Table 2
The parameters of the constituent elements in HEAs [6,41].

Elements	Al	Fe	Ni	Mn	Cu
Atomic radius (pm)	143.2	124.1	124.6	126.4	127.8
Melting point (K)	933	1811	1728	1519	1358
Density (g/cm ³)	2.70	7.88	8.91	7.47	8.94

Table 3
The mixing enthalpy (kJ/mol) [42,43] is calculated with reference to Miedema theory.

Elements	Al	Fe	Ni	Mn	Cu
Al	—	-11	-22	-19	-1
Fe	—	—	-2	0	13
Ni	—	—	—	-8	4
Mn	—	—	—	—	4
Cu	—	—	—	—	—

disordered BCC phases based on the inverse fast Fourier transform (IFFT) in Fig. 3(d). As illustrated in Fig. 3(e), the EDS maps reveal a significant segregation of Fe, suggesting a poor binding between Fe and other elements [44]. For Cu1.25, the magnified regions of Fig. 4(a) illustrate shorter and fewer rod-like precipitates of BCC structures based on the SAED (Fig. 4(b)), indicating a reduction in BCC phases. Additionally, the large sizes of numerous strip-like precipitates are observed, which can be divided into two main categories, Cu-rich and Fe-rich (see in Fig. 4(e)). Furthermore, the Cu-rich and Fe-rich precipitates are identified as FCC1 and FCC2 structures based on SAED (Fig. 4(c-d)) corresponding to the emergence of two diffraction peaks of FCC1 and FCC2 in the XRD result. Additionally, it can be concluded that Mn element is homogeneously distributed.

Thermodynamic properties are the crucial factor in the formation of solid solutions and intermetallic compounds within HEAs [9,45]. A review of the literature reveals that the rules of the stabilized solid solutions [8,46,47], namely $-22 \leq \Delta H_{mix} \leq 7$ kJ/mol, $-11 \leq \Delta S_{mix} \leq 19.5$ J/(mol·K), $\delta \leq 6.6\%$, $\Omega \geq 1.1$ have been established. The thermodynamic values are calculated based on the available literature [47–49]. As illustrated in Table 4, the mixing entropy (ΔS_{mix}), the mixing enthalpy (ΔH_{mix}), the entropy-enthalpy ratio (Ω) and the atomic size difference (δ) of the studied HEAs meet the criteria for the formation of the stable solid solution, which rationalizes the experimental results. Additionally, the valence electron concentration (VEC) is found to exert a significant effect on the stability of phases [47]. The VEC rule has recently been revised to BCC: $VEC \leq 6.87$ and FCC: $VEC \geq 8.0$. Two FCC + BCC phases are stable between 6.87 and 8.0. However, the Cu0.5 do not comply with the empirical criteria of VEC, indicating the presence of

a few FCC phases that are not detected by XRD. Similar phenomena occur in the investigated AlCrCuFeMnNi and CrCuFeMnNi systems [50, 51].

3.2. Mechanical properties

According to the principles of crystallography, single-phase BCC structural materials exhibit superior strength but inferior plasticity in comparison to materials with FCC structure [41,52]. The compression experiment was conducted three times (see in Figs. S2–S4 and Tables S2–S4). Fig. 5(a-b) illustrates representative outcomes of the compression test and HRTEM images of Cu1.25 at grain boundaries. As illustrated in Table 5, it is evident that the fracture strength of Cu1.0 is 24 % higher than that of Cu0.5. Additionally, the yield strength and the plastic strain increase from 1291 MPa and 10.2 % to 1559 MPa and 14.3 %, respectively. The compression results are more favorable than other Cu-containing HEAs that have been investigated, including CoCrFeMnNiCu, AlFeNiMnCuTi and AlFeNiMnCuCr systems [25,26,53, 54]. This indicates that the Cu1.0 possesses high strength with enhanced plasticity. These observations can be attributed to the strengthening of the B2 phases increases and the severe lattice distortion (see in Table S1), which inhibits the transfer of dislocation during deformation [27,55]. However, there is a decline in both compressive strength and plasticity when $x = 1.25$, which is attributed to the aggregation of defects and dislocations at grain boundaries leading to the superposition of the stress field (see in Fig. 5(b)), as well as the formation of complex Fe/Cu-rich precipitates of FCC structures. Furthermore, while Cu contents differ among the samples, the four compressive stress-strain curves exhibit a similar feature: a displacement burst occurred at the yield point. This phenomenon is associated with the formation of local cracks [56], which may be attributed to the inadequate displacement feedback during the burst events, as previously discussed in the literature [57,58]. And the impact is more pronounced in smaller samples [59].

The hardness and density experiments were conducted five times (see in Tables S5–S6), and Fig. 5(c) illustrates representative outcomes. Fig. 5(c) shows the high hardness of the HEAs, which is attributed to the BCC structure. Explanations for this phenomenon have been mentioned several occasions in Al-containing HEAs, including AlFeNiMnCrCu0.5 (518 HV) [26], AlFeCoMnCu (463 HV) [41], Al₂CoCrFeNiCu (73 HRA) [24]. This phenomenon can be due to the inherent stability of the BCC structure. And the Vickers hardness of the HEAs is superior to that of quite a lot of Cu-containing HEAs [2,41,44,60]. However, as Cu content increased further, the hardness decreases due to the conversion of BCC structures into FCC structures when $x = 1.25$ [26]. Additionally, the density of the HEAs increases due to the addition of Cu element with high-density.

Secondary electron mode (SEM) images of the fracture surface morphology are presented in Fig. 6. As illustrated in Fig. 6(a), numerous

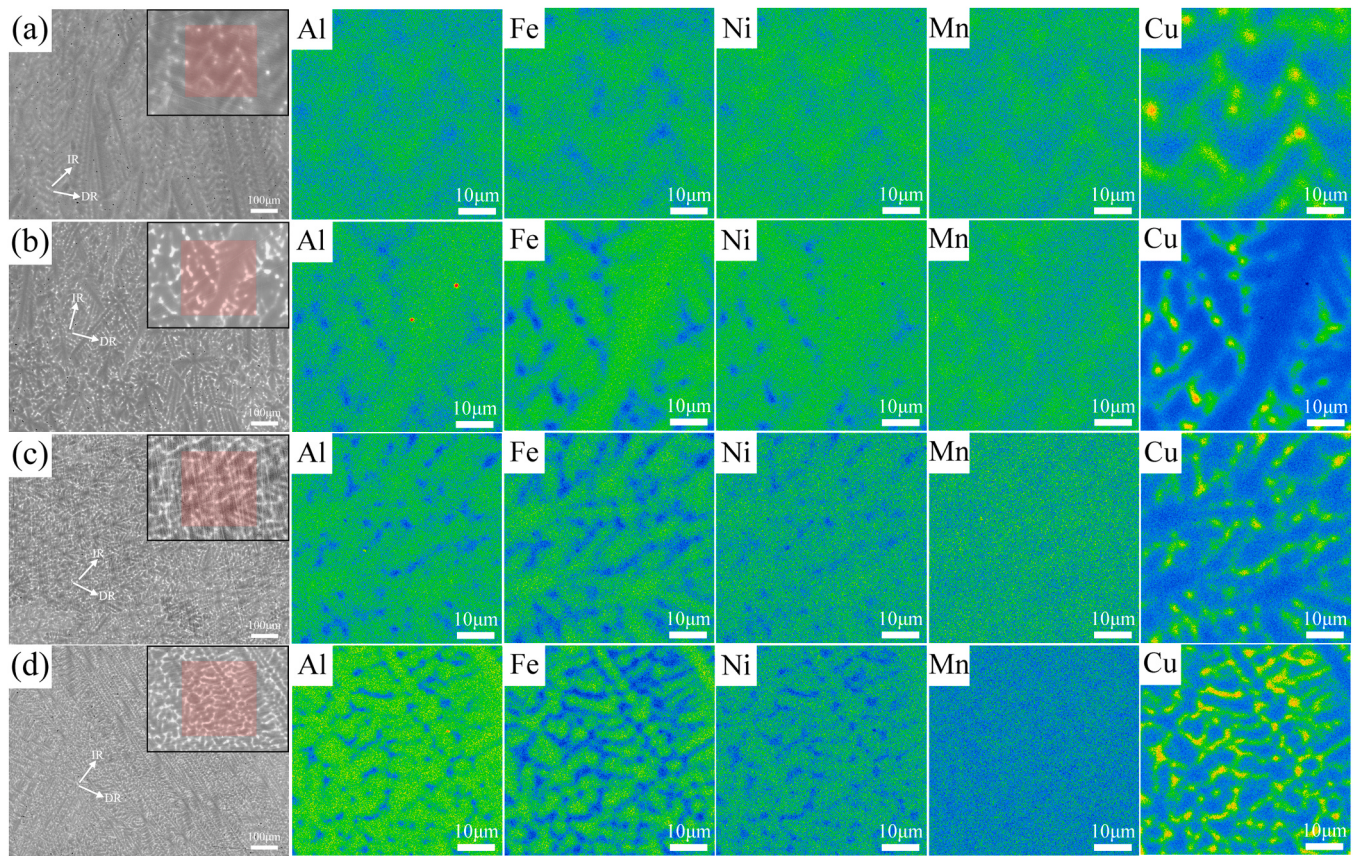


Fig. 2. The BSE images and WDS maps: (a) Cu0.5, (b) Cu0.75, (c) Cu1.0, (d) Cu1.25.

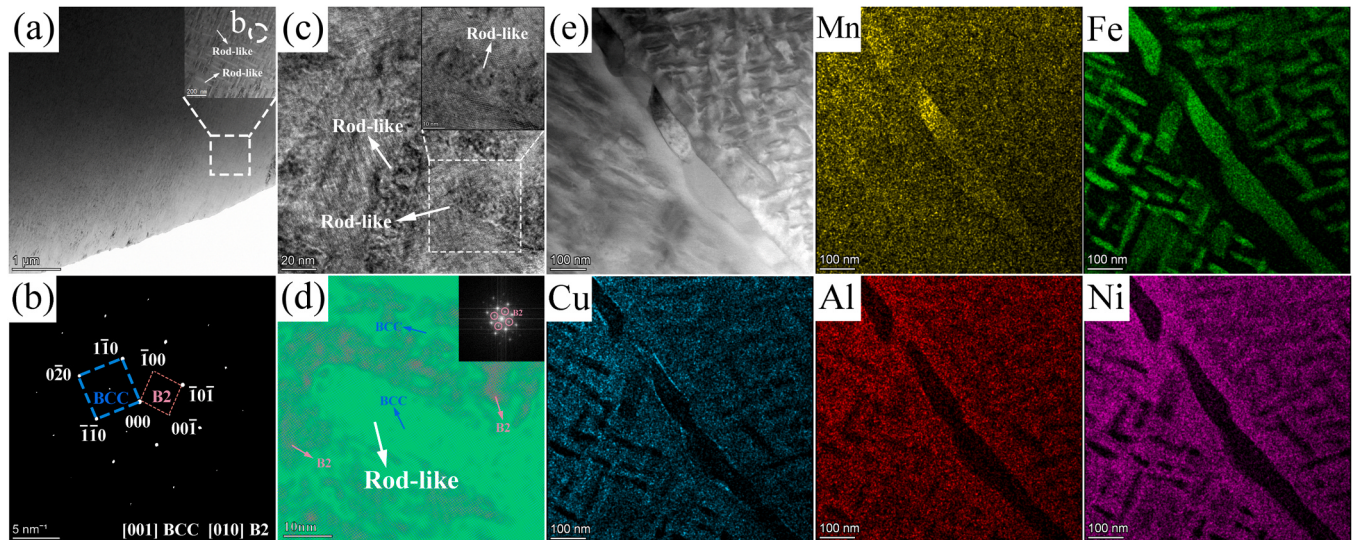


Fig. 3. The TEM results of Cu0.5: (a) TEM micrograph, (b) SAED results of white circles, (c-d) HRTEM image and IFFT image corresponding to B2 structure, (e) EDS maps.

cleavage steps are observed on the surface of Cu0.5, which indicates that the compression fracture pattern exhibits a brittle cleavage fracture, similar to that observed in single-phase BCC HEAs [61]. In Fig. 6(b), the fracture surface exhibits typical intergranular fractures, displaying river-like patterns and cleavage steps at varying parallel heights. Additionally, the dimensions of the fracture features on the surface are markedly smaller than those observed in Cu0.5 [62]. Fig. 6(c) displays high-density and

long tear edges, which are identified as quasi-cleavage fractures, indicating an increase in plasticity for Cu1.0. While for the Cu1.25 (Fig. 6(d)), the fracture surface features exhibit both brittle and ductile fracture characteristics, including disordered river-like patterns, cleavage steps and dimples. These features are attributed to the precipitation of complex FCC phases, which resulted in a reduction in mechanical properties.

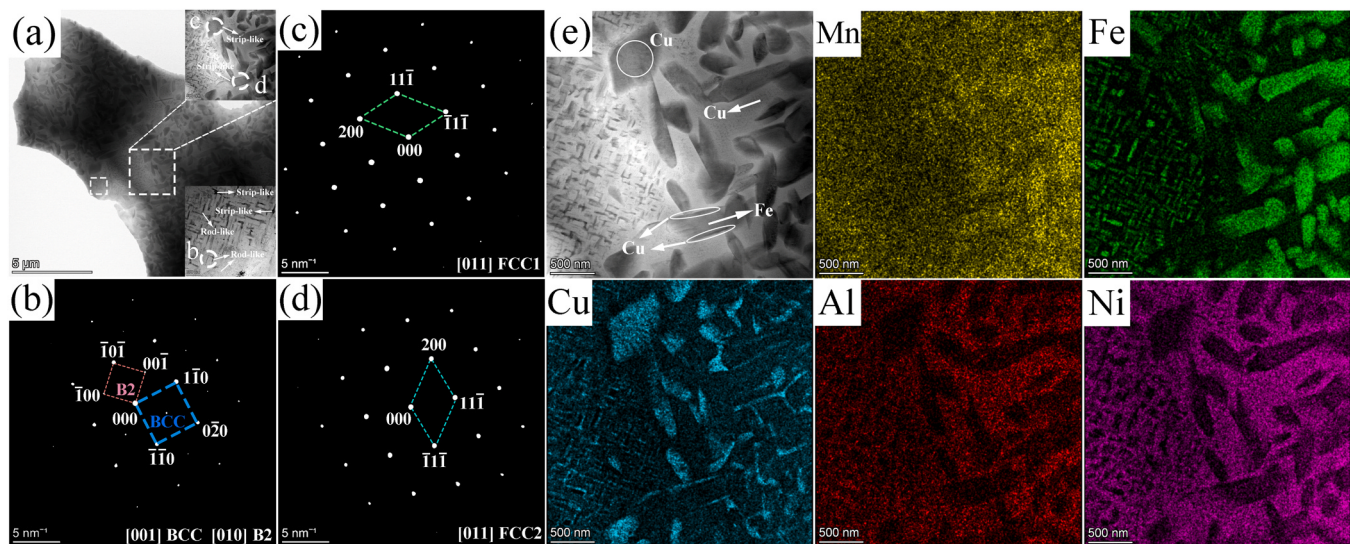


Fig. 4. The TEM results of Cu1.25: (a) TEM micrograph, (b-d) SAED results of white circles, (e) EDS maps.

Table 4
The thermodynamic parameter.

Alloys	ΔS_{mix} (J/ mol•K)	ΔH_{mix} (kJ/ mol)	δ (%)	Ω	VEC	Phases
Cu0.5	13.15	-14.61	5.39	1.33	7.44	BCC+B2
Cu0.75	13.33	-12.52	5.26	1.56	7.63	BCC+B2+FCC1
Cu1.0	13.38	-10.77	5.14	1.83	7.80	BCC+B2+FCC1+FCC2
Cu1.25	13.35	-9.28	5.03	2.10	7.95	BCC+B2+FCC1+FCC2

3.3. Corrosion resistance

The electrochemical corrosion experiment was conducted three times (see in Figs. S5–S7 and Tables S7–S9). Representative results of corrosion behavior are illustrated in Fig. 7. The corrosion potential (E_{corr}) and corrosion current (I_{corr}) are obtained from the potentiodynamic polarization curves, as presented in Table 6. As illustrated in Fig. 7(a), the potentiodynamic polarization curves exhibits a transition platform, which indicates the occurrence of passivation. Passivation is defined as the formation of a dense passive film on the surface under specific conditions during electrochemical corrosion. Table 6 indicates

that the change in Cu content has a significant impact on the corrosion resistance. Previous studies have demonstrated that the E_{corr} has a positive correlation with the stability of HEAs in corrosive solution, and the I_{corr} is inversely proportional to corrosion resistance [63]. Notably, Cu1.0 has the lowest I_{corr} ($22.7 \mu\text{A}/\text{cm}^2$), which suggests that the corrosion rate is reduce with increasing Cu content. Additionally, Cu1.25 exhibited the lowest E_{corr} (600 mV), indicating the Cu1.25 displays good chemical stability in 3.5 wt% NaCl solution. Fig. 7(b) illustrates the outcomes of the resistance of products film based on Nyquist plots (inline graph is an overall comparison). As the concentration of Cu increases, a decline in corrosion resistance is initially observed, followed by an enhancement. The Cu0.75 exhibits small semi-circle diameter with a high I_{corr} , indicating the possibility of pitting corrosion. From a

Table 5
Values of yield strength, fracture strength and plastic strain for the HEAs.

Alloys	Yield strength (MPa)	Fracture strength (MPa)	Plastic strain (%)
Cu0.5	1291 ± 181	1371 ± 191	10.2 ± 0.5
Cu0.75	1492 ± 54	1640 ± 14	13.0 ± 1.4
Cu1.0	1559 ± 92	1699 ± 111	14.3 ± 1.0
Cu1.25	1388 ± 183	1531 ± 221	12.1 ± 0.4

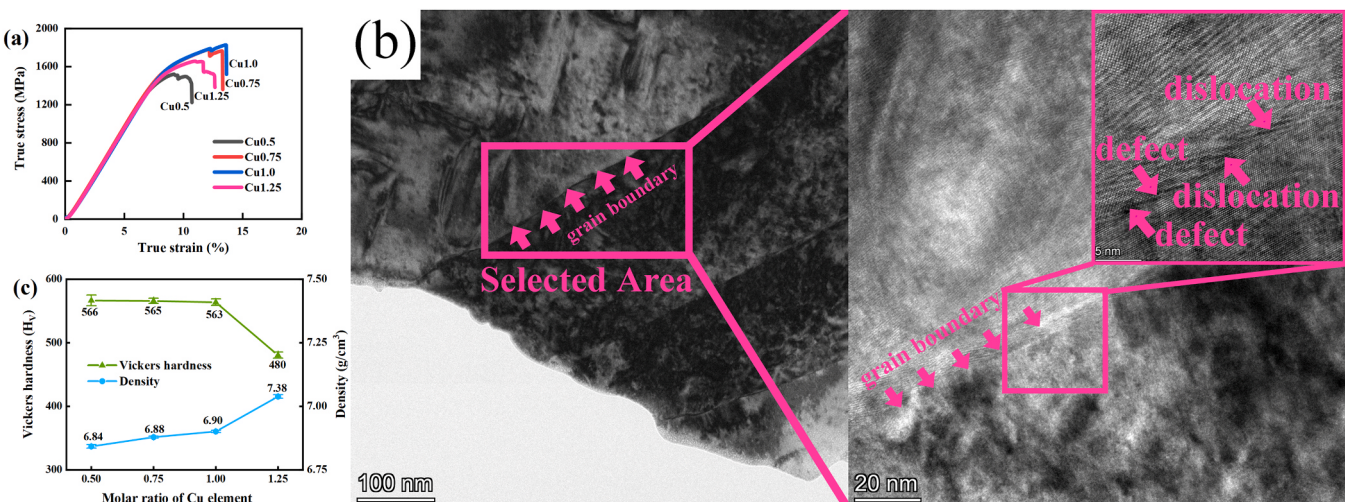


Fig. 5. (a) Compression results, (b) HRTEM images of Cu1.25 and (c) Values of Vickers hardness and density.

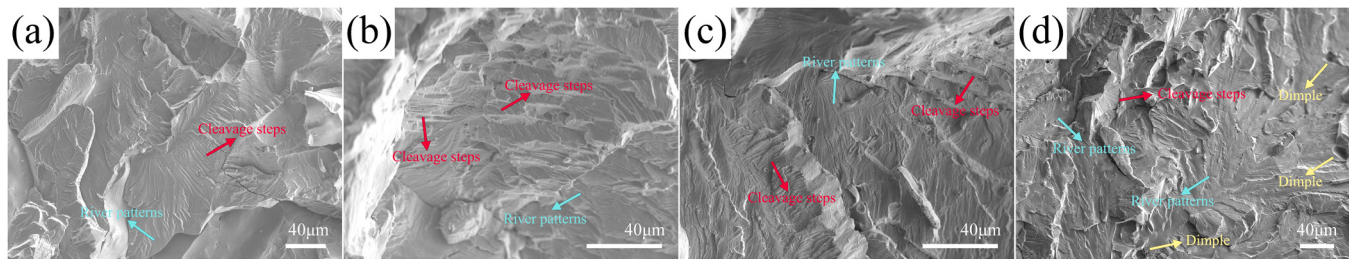


Fig. 6. SEM images of fracture surface: (a) Cu0.5, (b) Cu0.75, (c) Cu1.0, (d) Cu1.25.

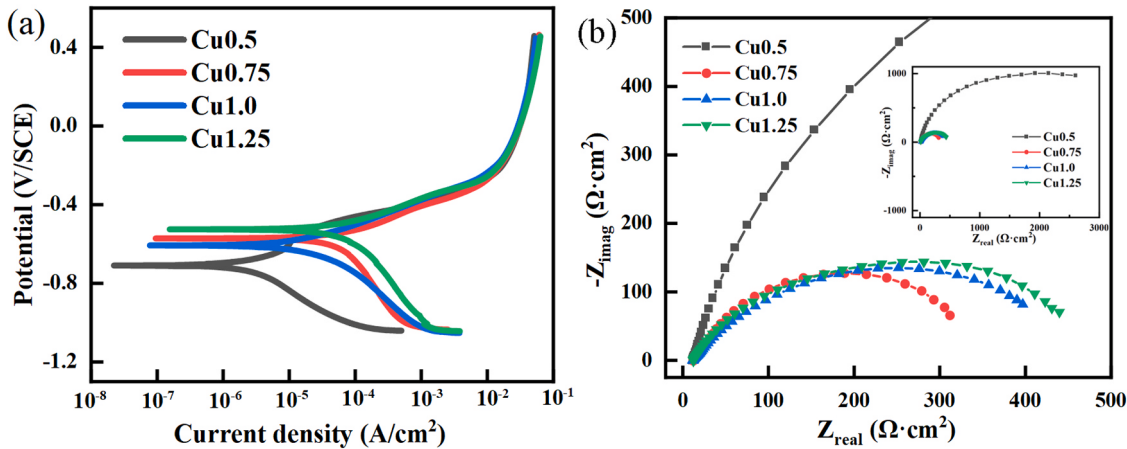


Fig. 7. (a) Potentiodynamic polarization curves and (b) Nyquist plots.

Table 6
Electrochemical parameters of the HEAs.

Alloys	E_{corr} (mV)	I_{corr} ($\mu A/cm^2$)
Cu0.5	-639.5 ± 81.5	31.2 ± 2.0
Cu0.75	-704.9 ± 123.3	74.9 ± 16.6
Cu1.0	-678.5 ± 65.1	22.7 ± 2.9
Cu1.25	-600.3 ± 97.6	35.1 ± 1.0

holistic perspective, the addition of Cu is advantageous in improving the stability of the HEAs in 3.5 wt% NaCl solution and also in reducing the corrosion rate. Additionally, the corrosion results of the HEAs are more favorable than several Cu-containing HEAs, including AlFeCoMnCu [41], AlCoCrFeNiCu [64].

The surface morphologies after corrosion are presented in Fig. 8. As illustrated in Fig. 8(a), the observation of corrosion grooves and a multitude of pits indicates the possibility of pitting corrosion. Furthermore, numerous long and deep grooves are linked by a network of adjacent pits, which is indicative of pitting corrosion being the predominant corrosion mechanism in B2-HEAs [65]. As the Cu content increased, the appearance of deep and long pits on the surface of Cu0.75 is observed (see in Fig. 8(b)), which is attributed to the increase of B2

phases. For Cu1.0, in contrast to pitting corrosion, the formation of block-like holes are observed in Fig. 8(c), which suggests the transformation of corrosion mechanism, eased the pitting corrosion. As illustrated in Fig. 8(d), the visible phase corrosion is observed in the IR, corresponding to the BSE images. This phenomenon can be attributed to the precipitation of complex FCC phases when $x = 1.25$, resulting in a distinct potential between the DR and the IR, caused by the distribution of the non-homogenous composition [41].

4. Conclusions

Microstructure, mechanical and corrosion behavior of AlFeNiMnCu_x HEAs through vacuum arc melting have been investigated. The findings of the study revealed that the effect of an increase in the Cu content on the microstructure and properties. First of all, the formation of B2 compounds is related to the substitutional solid solution theory and enhances the mechanical properties. Additionally, the addition of Cu tends to cause HEAs to form FCC structures, which weakens the mechanical properties while altering the electrochemical corrosion mode, thus slowing the corrosion rate.

This work demonstrates that an increase in Cu content has a significant impact on the HEAs, which contributes to improved mechanical

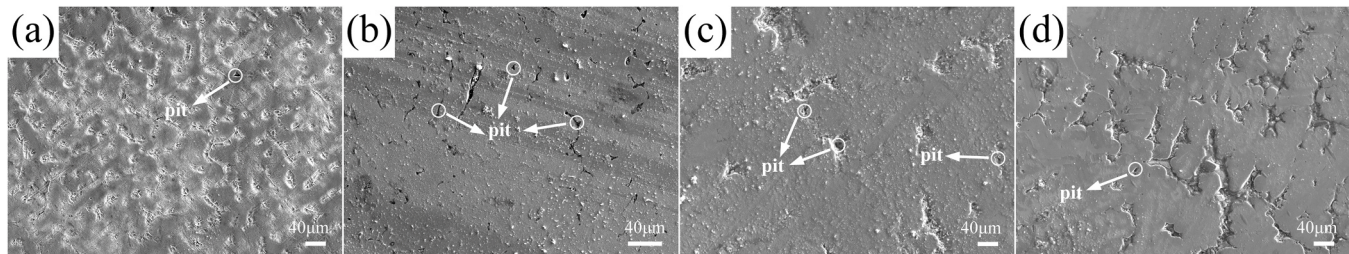


Fig. 8. The surface morphology after corrosion: (a) Cu0.5, (b) Cu0.75, (c) Cu1.0, (d) Cu1.25.

properties and corrosion resistance. These findings will offer valuable insights for the development of Cu-containing HEAs.

CRediT authorship contribution statement

Zhao Linjiansheng: Writing – review & editing, Writing – original draft, Methodology, Investigation, Formal analysis, Data curation. **Xu Chenran:** Writing – review & editing, Data curation. **Fang Liyang:** Writing – review & editing, Formal analysis. **Tang Hongqun:** Writing – review & editing. **Ouyang Yifang:** Writing – review & editing, Funding acquisition. **Tao Xiaoma:** Writing – review & editing, Funding acquisition, Conceptualization.

Declaration of Competing Interest

The authors declared that they have no known competing financial interests or personal relationships that could have appeared to influence the work reported in this paper.

Acknowledgments

This work is financially supported by the Guangxi Science and Technology Major Program (No. AA23073019) and National Natural Science Foundation of China (51961007, 12364001).

Appendix A. Supporting information

Supplementary data associated with this article can be found in the online version at [doi:10.1016/j.jallcom.2025.180124](https://doi.org/10.1016/j.jallcom.2025.180124).

Data availability

The data that support the findings of this study are available on request from the corresponding author. The data are not publicly available due to privacy or ethical restrictions.

References

- [1] J.W. Yeh, S.K. Chen, S.J. Lin, J.Y. Gan, T.S. Chin, T.T. Shun, C.H. Tsau, S.Y. Chang, Nanostructured high-entropy alloys with multiple principal elements: novel alloy design concepts and outcomes, *Adv. Eng. Mater.* 6 (2004) 299–303.
- [2] Y. Zhang, T.T. Zuo, Z. Tang, M.C. Gao, K.A. Dahmen, P.K. Liaw, Z.P. Lu, Microstructures and properties of high-entropy alloys, *Prog. Mater. Sci.* 61 (2014) 1–93.
- [3] J.W. Yeh, Alloy Design strategies and future trends in high-entropy alloys, *JOM* 65 (2013) 1759–1771.
- [4] B. Cantor, I. Chang, P. Knight, A. Vincent, Microstructural development in equiatomic multicomponent alloys, *Mater. Sci. Eng.: A* 375 (2004) 213–218.
- [5] I. Toda-Caraballo, P. Rivera-Diaz-del-Castillo, A criterion for the formation of high entropy alloys based on lattice distortion, *Intermetallics* 71 (2016) 76–87.
- [6] D.B. Miracle, O.N. Senkov, A critical review of high entropy alloys and related concepts, *Acta Mater.* 122 (2017) 448–511.
- [7] S. Guo, Q. Hu, C. Ng, C.T. Liu, More than entropy in high-entropy alloys: Forming solid solutions or amorphous phase, *Intermetallics* 41 (2013) 96–103.
- [8] X. Yang, Y. Zhang, Prediction of high-entropy stabilized solid-solution in multi-component alloys, *Mater. Chem. Phys.* 132 (2012) 233–238.
- [9] M. Murali, S. Babu, B.J. Krishna, A. Vallimanaian, Synthesis and characterization of AlCoCrCuFeZn_x high-entropy alloy by mechanical alloying, *Prog. Nat. Sci.* 26 (2016) 380–384.
- [10] J.B. Cheng, X.B. Liang, B.S. Xu, Effect of Nb addition on the structure and mechanical behaviors of CoCrCuFeNi high-entropy alloy coatings, *Surf. Coat. Technol.* 240 (2014) 184–190.
- [11] Y. Xin, S.H. Li, Y.Y. Qian, W.K. Zhu, H.B. Yuan, P.Y. Jiang, R.H. Guo, L.B. Wang, High-entropy alloys as a platform for catalysis: progress, challenges, and opportunities, *ACS Catal.* 10 (2020) 11280–11306.
- [12] F. Otto, N.L. Hanold, E.P. George, Microstructural evolution after thermomechanical processing in an equiatomic, single-phase CoCrFeMnNi high-entropy alloy with special focus on twin boundaries, *Intermetallics* 54 (2014) 39–48.
- [13] B.E. MacDonald, Z.Q. Fu, X. Wang, Z.M. Li, W.P. Chen, Y.Z. Zhou, D. Raabe, J. Schoenung, H. Hahn, E.J. Lavernia, Influence of phase decomposition on mechanical behavior of an equiatomic CoCuFeMnNi high entropy alloy, *Acta Mater.* 181 (2019) 25–35.
- [14] V.R. Rocha, J.P. Cesare, T.C. Messina, Searching for magnetic high entropy alloy treasure in CoCr₂FeNiQ_y, *Intermetallics* 146 (2022) 107581.
- [15] J.Y. Yu, R.D. Mu, S.Y. Qu, Y. Cai, Z.Y. Shen, The effect of heat treatment at 1200 °C on microstructure and mechanical properties evolution of AlCoCrFeNiSiYHF high entropy alloys, *Vacuum* 200 (2022) 111039.
- [16] S.H. Shim, H. Pouraliakbar, B.J. Lee, Y.K. Kim, M.S. Rizi, J.H. Han, S.I. Hong, Supporting data for strengthening and deformation behavior of as-cast CoCrCu_{1.5}MnNi high entropy alloy with micro-/nanoscale precipitation, *Data Brief.* 45 (2022) 108567.
- [17] W. Qi, W.R. Wang, X. Yang, G.N. Zhang, W. Ye, Y.T. Su, Y. Li, S.Y. Chen, Effects of Al and Ti co-doping on the strength-ductility- corrosion resistance of CoCrFeNi-AlTi high-entropy alloys, *J. Alloy. Compd.* 925 (2022) 166751.
- [18] H. Luo, S. Zou, Y. Chen, Z. Li, C. Du, X. Li, Influence of carbon on the corrosion behaviour of interstitial equiatomic CoCrFeMnNi high-entropy alloys in a chlorinated concrete solution, *Corros. Sci.* 163 (2020) 108287.
- [19] G. Qin, R. Chen, H. Zheng, H. Fang, L. Wang, Y. Su, J. Guo, H. Fu, Strengthening FCC-CoCrFeMnNi high entropy alloys by Mo addition, *J. Mater. Sci. Technol.* 35 (2019) 578–583.
- [20] M.V. Klimova, D.G. Shaysultanov, S.V. Zherebtsov, N.D. Stepanov, Effect of second phase particles on mechanical properties and grain growth in a CoCrFeMnNi high entropy alloy, *Mater. Sci. Eng.: A* 748 (2019) 228–235.
- [21] W.R. Wang, W.L. Wang, S.C. Wang, Y.C. Tsai, C.H. Lai, J.W. Yeh, Effects of Al addition on the microstructure and mechanical property of Al_xCoCrFeNi high-entropy alloys, *Intermetallics* 26 (2012) 44–51.
- [22] J.Y. He, W.H. Liu, H. Wang, Y. Wu, X.J. Liu, T.G. Nieh, Z.P. Liu, Effects of Al addition on structural evolution and tensile properties of the FeCoNiCrMn high-entropy alloy system, *Acta Mater.* 62 (2014) 105–113.
- [23] Z. Rao, X. Wang, Q. Wang, T. Liu, X. Chen, L. Wang, X. Hui, Microstructure, mechanical properties, and oxidation behavior of Al_xCr_{0.4}CuFe_{0.4}MnNi high entropy alloys, *Adv. Eng. Mater.* 19 (2017) 1600726.
- [24] Y.Y. Liu, Z. Chen, J.C. Shi, Z.Y. Wang, J.Y. Zhang, The effect of Al content on microstructures and comprehensive properties in Al_xCoCrCuFeNi high entropy alloys, *Vacuum* 161 (2019) 143–149.
- [25] V.A.S. Kondapalli, K. Suresh, M. Ramakrishna, N. Narasiah, B. Srinivasarao, Effect of Cu content on the microstructure and mechanical properties of FeNiMnCuAl_{0.1}Ti_{0.1} ($x=0.5, 1.0$ and 1.5) high entropy alloy system, *J. Alloy. Compd.* 940 (2023) 168819.
- [26] N. Thanhung, M. Huang, H. Li, L. Hong, S. Yang, Effect of Al content on microstructure and mechanical properties of as-cast Al_xFeMnNiCrCu_{0.5} high-entropy alloys, *Mater. Sci. Eng.: A* 832 (2022) 142495.
- [27] R. Guo, J. Pan, L. Liu, Achieving dual-phase structure and improved mechanical properties in AlCoCrFeTiO_{0.5} high-entropy alloys by addition of Ni, *Mater. Sci. Eng.: A* 831 (2022) 142194.
- [28] X.F. Wang, Y. Zhang, Y. Qiao, G.L. Chen, Novel microstructure and properties of multicomponent CoCrCuFeNiTix alloys, *Intermetallics* 15 (2007) 357–362.
- [29] H. Nam, S. Park, S.W. Kim, S.H. Shim, Y. Na, N. Kim, S. Song, S.I. Hong, N. Kang, Enhancement of tensile properties applying phase separation with Cu addition in gas tungsten arc welds of CoCrFeMnNi high entropy alloys, *Scr. Mater.* 220 (2022) 114897.
- [30] B. Gwalani, D. Choudhuri, V. Soni, Y. Ren, M. Styles, J.Y. Hwang, S.J. Nam, H. Ryu, S.H. Hong, R. Banerjee, Cu assisted stabilization and nucleation of L₁ precipitates in Al_{0.3}CuFeCrNi₂ fcc-based high entropy alloy, *Acta Mater.* 129 (2017) 170–182.
- [31] J. Wang, H. Jiang, X. Chang, L. Zhang, H. Wang, L. Zhu, S. Qin, Effect of Cu content on the microstructure and corrosion resistance of AlCrFeNi₃Cu_x high entropy alloys, *Corros. Sci.* 221 (2023) 11313.
- [32] S.S. Nene, M. Frank, K. Liu, S. Sinha, R.S. Mishra, B.A. McWilliams, K.C. Cho, Corrosion-resistant high entropy alloy with high strength and ductility, *Scr. Mater.* 166 (2019) 168–172.
- [33] B. Yang, Y. Hou, Q. Lei, Y. Li, A. Chiba, Influence of Cu addition on corrosion behavior and tensile performance of Ni-30Co-16Cr-15Mo-6Fe alloy, *Mater. Charact.* 161 (2020) 110140.
- [34] H.Y. Chen, C.W. Tsai, C.C. Tung, J.W. Yeh, T.T. Shun, C.C. Yang, S.K. Chen, Effect of the substitution of Co by Mn in Al-Cr-Cu-Fe-Co-Ni high-entropy alloys, *Ann. Chim. Sci. Mater.* 31 (2006) 685–698.
- [35] F. Otto, A. Dlouhy, K.G. Pradeep, M. Kubanova, D. Raabe, G. Eggeler, E.P. George, Decomposition of the single-phase high-entropy alloy CrMnFeCoNi after prolonged anneals at intermediate temperatures, *Acta Mater.* 112 (2016) 40–52.
- [36] E.J. Pickering, R. Munoz-Moreno, H.J. Stone, N.G. Jones, Precipitation in the equiatomic high-entropy alloy CrMnFeCoNi, *Scr. Mater.* 113 (2016) 106–109.
- [37] B. Schuh, F. Mendez-Martin, B. Voelker, E.P. George, H. Clemens, R. Pippan, A. Hohenwarter, Mechanical properties, microstructure and thermal stability of a nanocrystalline CoCrFeMnNi high-entropy alloy after severe plastic deformation, *Acta Mater.* 96 (2015) 258–268.
- [38] A. Verma, P. Tarate, A.C. Abhyankar, M.R. Mohape, D.S. Gowtam, V.P. Deshmukh, T. Shanmugasundaram, High temperature wear in CoCrFeNiCu_x high entropy alloys: the role of Cu, *Scr. Mater.* 161 (2019) 28–31.
- [39] C. Meng, Z.H. Song, X.W. Qiu, G.L. Wang, C. Wu, X. Ren, W.B. Zhuang, X.L. Wang, Effect of Cu content on microstructure and properties of CoCrFeNiCu_x high-entropy alloy coatings prepared by induction cladding, *J. Alloy. Compd.* 934 (2023) 167896.
- [40] Y. Yuan, J.J. Wang, J. Wei, W.Y. Chen, H.L. Yan, N. Jia, Cu alloying enables superior strength-ductility combination and high corrosion resistance of FeMnCoCr high entropy alloy, *J. Alloy. Compd.* 970 (2024) 172543.
- [41] Y. Yan, L. Fang, Y. Tan, X. Tao, Y. Ouyang, Y. Du, Mechanical properties and corrosion resistance of AlxCoCuFeMn high-entropy alloys, *J. Mater. Res. Technol.* 24 (2023) 5250–5259.

- [42] Y.P. Lu, H. Jiang, S. Guo, T.M. Wang, Z.Q. Cao, T.J. Li, A new strategy to design eutectic high-entropy alloys using mixing enthalpy, *Intermetallics* 91 (2017) 124–128.
- [43] F. Otto, Y. Yang, H. Bei, E.P. George, Relative effects of enthalpy and entropy on the phase stability of equiatomic high-entropy alloys, *Acta Mater.* 61 (2013) 2628–2638.
- [44] T. Guo, J. Li, J. Wang, Y. Wang, H. Kou, S. Niu, Liquid-phase separation in undercooled CoCrCuFeNi high entropy alloy, *Intermetallics* 86 (2017) 110–115.
- [45] A. Takeuchi, A. Inoue, Mixing enthalpy of liquid phase calculated by miedema's scheme and approximated with sub-regular solution model for assessing forming ability of amorphous and glassy alloys, *Intermetallics* 18 (2010) 1779–1789.
- [46] Y. Zhang, Y.J. Zhou, J.P. Lin, G.L. Chen, P.K. Liaw, Solid-solution phase formation rules for multi-component alloys, *Adv. Eng. Mater.* 10 (2008) 534–538.
- [47] S. Guo, C.T. Liu, Phase stability in high entropy alloys: formation of solid-solution phase or amorphous phase, *Prog. Nat. Sci.* 21 (2011) 433–446.
- [48] X.D. Xu, S. Guo, T.G. Nieh, C.T. Liu, A. Hirata, M.W. Chen, Effects of mixing enthalpy and cooling rate on phase formation of $\text{Al}_x\text{CoCrCuFeNi}$ high-entropy alloys, *Materialia* 6 (2019) 100292.
- [49] M.X. Ren, B.S. Li, H.Z. Fu, Formation condition of solid solution type high-entropy alloy, *T. Nonferr. Metal. Soc.* 23 (2013) 991–995.
- [50] S. Guo, C. Ng, J. Lu, C.T. Liu, Effect of valence electron concentration on stability of fcc or bcc phase in high entropy alloys, *J. Appl. Phys.* 109 (2011) 103505.
- [51] I. Alam, M.A. Adaan-Nyiak, A.A. Tiamiyu, Revisiting the phase stability rules in the design of high-entropy alloys: a case study of quaternary alloys produced by mechanical alloying, *Intermetallics* 159 (2023) 107919.
- [52] Y.J. Zhou, Y. Zhang, Y.L. Wang, G.L. Chen, Solid solution alloys of AlCoCrFeNiTi_x with excellent room-temperature mechanical properties, *Appl. Phys. Lett.* 90 (2007) 181904.
- [53] G. Ren, L. Huang, K. Hu, T. Li, Y. Lu, D. Qiao, H. Zhang, D. Xu, T. Wang, T. Li, P. K. Liaw, Enhanced antibacterial behavior of a novel Cu-bearing high-entropy alloy, *J. Mater. Sci. Technol.* 117 (2022) 158–166.
- [54] X. Xian, L. Lin, Z. Zhong, C. Zhang, C. Chen, K. Song, J. Cheng, Y. Wu, Precipitation and its strengthening of Cu-rich phase in CrMnFeCoNiCu_x high-entropy alloys, *Mater. Sci. Eng.: A* 713 (2018) 134–140.
- [55] R.R. Chen, G. Qin, H.T. Zheng, L. Wang, Y.Q. Su, Y.L. Chiu, H.S. Ding, J.J. Guo, H. Z. Fu, Composition design of high entropy alloys using the valence electron concentration to balance strength and ductility, *Acta Mater.* 144 (2018) 129–137.
- [56] N.D. Stepanov, N.Y. Yurchenko, V.S. Sokolovsky, M.A. Tikhonovsky, G. A. Salishchev, An $\text{AlNbTiVZr}_{0.5}$ high-entropy alloy combining high specific strength and good ductility, *Mater. Lett.* 161 (2015) 136–139.
- [57] D.M. Dimiduk, E.M. Nadgorny, C. Woodward, M.D. Uchic, P.A. Shafe, An experimental investigation of intermittent flow and strain burst scaling behavior in LiF crystals during microcompression testing, *Philos. Mag.* 90 (2010) 3621–3649.
- [58] D.M. Dimiduk, C. Woodward, R. LeSar, M.D. Uchic, Scale-free intermittent flow in crystal plasticity, *Science* 312 (2006) 1188–1190.
- [59] Y. Zou, S. Maiti, W. Steurer, R. Spolenak, Size-dependent plasticity in an $\text{Nb}_{25}\text{Mo}_{25}\text{Ta}_{25}\text{W}_{25}$ refractory high-entropy alloy, *Acta Mater.* 65 (2014) 85–97.
- [60] J.W. Yeh, S.Y. Chang, Y.D. Hong, S.K. Chen, S.J. Lin, Anomalous decrease in X-ray diffraction intensities of Cu-Ni-Al-Co-Cr-Fe-Si alloy systems with multi-principal elements, *Mater. Chem. Phys.* 103 (2007) 41–46.
- [61] N.N. Guo, L. Wang, L.S. Luo, X.Z. Li, Y.Q. Su, J.J. Guo, H.Z. Fu, Microstructure and mechanical properties of refractory MoNbHfZrTi high-entropy alloy, *Mater. Des.* 81 (2015) 87–94.
- [62] S.H. Chen, J.S. Zhang, S. Guan, T. Li, J.Q. Liu, F.F. Wu, Y.C. Wu, Microstructure and mechanical properties of WNbMoTaZr_x ($x=0.1, 0.3, 0.5, 1.0$) refractory high entropy alloys, *Mat. Sci. Eng.: A* 835 (2022) 142701.
- [63] S. Xia, Z. Xia, D. Zhao, Y. Xie, X. Liu, L. Wang, Microstructure formation mechanism and corrosion behavior of FeCrCuTiV two-phase high entropy alloy prepared by different processes, *Fusion Eng. Des.* 172 (2021) 112792.
- [64] S. Pratskova, O. Samoilova, E. Ageenko, N. Shaburova, A.O. Moghaddam, E. Trofimov, Corrosion resistance of $\text{Al}_x\text{CoCrFeNiM}$ ($M = \text{Ti}, \text{V}, \text{Si}, \text{Mn}, \text{Cu}$) high entropy alloys in NaCl and H_2SO_4 solutions, *Metals* 12 (2022) 352.
- [65] Z.J. Shi, Z.B. Wang, X.D. Wang, S. Zhang, Y.G. Zheng, Effect of thermally induced B2 phase on the corrosion behavior of an $\text{Al}_{0.3}\text{CoCrFeNi}$ high entropy alloy, *J. Alloy. Compd.* 903 (2022) 163886.